Whole-Body Diffusion Imaging Applying Simultaneous Multi-Slice Excitation

Ganzkörper diffusionsgewichtete Bildgebung bei gleichzeitiger Anregung mehrerer Schichten

Authors D. Kenkel[1], M. C. Wurnig[1], L. Filli[1], E. J. Ulbrich[1], V. M. Runge[2], T. Beck[3], A. Boss[1]

Affiliations
[1] Department of Diagnostic and Interventional Radiology, University Hospital Zurich, Switzerland
[2] Department of Neuroradiology, University Hospital Zurich, Switzerland
[3] Siemens Healthcare GmbH, Erlangen, Germany

Key words
- molecular imaging
- MR-diffusion/perfusion
- MR-functional imaging

received 4.9.2014
accepted 27.11.2015

Bibliography
DOI http://dx.doi.org/10.1055/s-0035-1567032
Published online: 27.1.2016
Fortschr Röntgenstr 2016; 188: 381–388 © Georg Thieme Verlag KG Stuttgart · New York · ISSN 1438-9029

Correspondence
David Kenkel
Diagnostische und Interventionelle Radiologie, Universitätsspital Zürich
Rämistrasse 100
CH-8091 Zürich
Switzerland
Tel.: ++41/44/2 55 36 77
Fax: ++41/44/2 55 44 43
david.kenkel@usz.ch

Zusammenfassung

Ziel: Ziel dieser Studie ist es, die Machbarkeit eines schnellen Protokolls für die diffusionsgewichtete Ganzkörper-Bildgebung unter Verwendung einer echoplanaren Sequenz mit zeitgleicher Anregung mehrerer Schichten zu untersuchen, welche bei vergleichbaren Aufnahmeparametern im Vergleich zu einer konventionellen Ganzkörper-Messung eine deutlich reduzierte Messzeit bietet.

Material und Methoden: Eine single-shot echoplanare Sequenz mit der Option, mehrere Schichten gleichzeitig anzuregen und auszulesen, wurde für die diffusionsgewichtete Ganzkörper-Bildgebung an einem 3 T MR-Tomografen optimiert. Ein vergleichbares Protokoll für Ganzkörper-Bildgebung unter Verwendung einer konventionellen Sequenz diente als Referenzstandard. Acht gesunde Individuen und ein onkologischer Patient wurden mittels diffusionsgewichteter Ganzkörper-Bildgebung untersucht. Die quantitative Analyse umfasste die Bestimmung des Diffusionskoeffizienten (ADC) und des zugehörigen Varianzkoeffizienten in unterschiedlichen Organen. Die Bildqualität wurde qualitativ durch zwei unabhängige Radiologen auf einer 4-Punkt-Likert-Skala bestimmt.

Ergebnisse: Mit dem optimierten Protokoll konnte die Messzeit um bis zu 25,9 % reduziert werden. Beide Protokolle, sowohl das Protokoll mit beschleunigter Schichtauslesung als auch das konventionelle Protokoll, zeigten vergleichbare Bildqualität ohne statistisch signifikante Unterschiede bei der Bildbeurteilung. Ebenso wurden keine signifikanten Unterschiede der ADC-Werte der parenchymatösen Organe gefunden, wohingegen die Diffusionskoeffizienten im Gehirn im beschleunigten Protokoll etwas höher waren im Vergleich zur Referenzmethode.

Schlussfolgerung: Es konnte gezeigt werden, dass echoplanare Sequenzen mit beschleunigter Schichtakquisition für die diffusionsgewichtete Ganzkörperbildgebung genutzt werden können und das

Abstract

Purpose: The purpose of this study was to examine the feasibility of a fast protocol for whole-body diffusion-weighted imaging (WB-DWI) using a slice-accelerated echo-planar sequence, which, when using comparable image acquisition parameters, noticeably reduces measurement time compared to a conventional WB-DWI protocol.

Materials and Methods: A single-shot echo-planar imaging sequence capable of simultaneous slice excitation and acquisition was optimized for WB-DWI on a 3 T MR scanner, with a comparable conventional WB-DWI protocol serving as the reference standard. Eight healthy individuals and one oncologic patient underwent WB-DWI. Quantitative analysis was carried out by measuring the apparent diffusion coefficient (ADC) and its coefficient of variation (CV) in different organs. Image quality was assessed qualitatively by two independent radiologists using a 4-point Likert scale.

Results: Using our proposed protocol, the scan time of the WB-DWI measurement was reduced by up to 25.9 %. Both protocols, the slice-accelerated protocol and the conventional protocol, showed comparable image quality without statistically significant differences in the reader scores. Similarly, no significant differences of the ADC values of parenchymal organs were found, whereas ADC values of brain tissue were slightly higher in the slice-accelerated protocol.

Conclusion: It was demonstrated that slice-accelerated DWI can be applied to WB-DWI protocols with the potential to greatly reduce the required measurement time, thereby substantially increasing clinical applicability.

Key Points
- Whole-body diffusion-weighted imaging (WB-DWI) using simultaneous multi-slice and blipped-CAIPIRINHA reduces the measurement time strongly without having a significant impact on image quality.

This document was downloaded for personal use only. Unauthorized distribution is strictly prohibited.

Potential besitzen, die benötigte Messzeit drastisch zu verkürzen und somit die klinische Anwendbarkeit der Ganzkörperbildgebung zu steigern.

Kernaussagen

- Die Ganzkörper-diffusionsgewichtete Bildgebung mit simultaneous multi-slice und blipped-CAIPIRINHA-Technik reduziert die Messzeit stark ohne einen signifikanten Einfluss auf die Bildqualität.
- Diese Reduktion trägt zur klinischen Anwendbarkeit der Ganzkörper diffusionsgewichteten MRT bei.
- Weitere Verbesserungen der slice-accelerated EPI-Sequence sind jedoch nötig und die Anwendung dieser Technik für onkologische Patienten bedarf einer weiteren Evaluierung in klinischen Studien.

- The reduction in measurement time might strongly contribute to the clinical applicability of WB-DWI.
- However, further refinement of the slice-accelerated EPI sequence, and the WB-DWI protocol applying this sequence type seems necessary; and the value of such WB-DWI protocols for assessment of systemic oncological diseases needs to be investigated in further clinical studies.

Citation Format:

- Kenkel D, Wurnig MC, Filli L et al. Whole-Body Diffusion Imaging Applying Simultaneous Multi-Slice Excitation. Fortschr Röntgenstr 2016; 188: 381–388

Introduction

Whole-body diffusion-weighted imaging (WB-DWI) is one of the most promising diagnostic techniques for the assessment of systemic oncological diseases such as malignant lymphoma (1), myeloma (2), melanoma (3), thyroid cancer (4), colorectal cancer (5), and uterine and cervical carcinoma (6). WB-DWI has attracted attention as a promising alternative to 18F-fluorodeoxyglucose (18F-FDG) positron emission tomography (PET) in many malignant diseases [1, 2, 4, 7 – 11]. The implementation of WB-DWI as a clinical tool in the management of oncological patients for initial disease staging and assessment of treatment response is, however, hampered by the relatively long measurement time, on the order of 30 – 60 minutes for a complete data set, which is likely a primary reason for its low utilization in daily clinical routine.

Within recent years, many new MRI acquisition techniques have been developed, allowing for a notable reduction of measurement time. One of the most promising approaches for diffusion-weighted imaging (DWI), in terms of reduced acquisition time, is the implementation of multi-slice excitation and acquisition, also known as "simultaneous multi-slice" (SMS) or "slice-accelerated imaging" [12]. Typically, in DWI one slice alone undergoes 2D spin excitation with subsequent data readout using an echo-planar imaging (EPI) strategy. The idea of slice-accelerated pulse sequences is to apply multiband (MB) composite RF pulses with a slice selection gradient to simultaneously excite multiple slice planes. Using a conventional EPI readout, the simultaneously excited slice would result in image aliasing; therefore, advanced readout techniques are applied, which use the different sensitivity of the receiver coil array to de-alias the images from different slices. Recently, the "controlled aliasing in parallel imaging results in higher acceleration" (CAIPIRINHA) technique [13] was introduced to separate slices with reduced g-factor penalty. Subsequently, Setsompop et al. [14] modified this technique and introduced a blip strategy that balances the blips applied to slices to minimize the voxel tilting artifact. The blips are applied simultaneously with the EPI phase-encoding blips and create inter-slice image shifts in the phase-encoding direction. However, this technique has not yet been used for WB-DWI, although there have been promising results, e. g., for the liver [15].

In this paper, we examine the hypothesis that an EPI sequence capable of simultaneous image acquisition can be applied to WB-DWI and will achieve similar image quality compared to conventional WB-DWI protocols with a notable reduction of measurement time. The hypothesis was tested in eight healthy volunteers; preliminary data on clinical applicability was obtained in one oncological patient.

Material and Methods

Subjects

In this prospective study, eight healthy volunteers were included (age range: 25 to 42 years; mean age: 30.1 years; all male), as well as one patient with metastatic renal cell carcinoma (74 years old, male). This study was performed with the approval of the local ethics committee. All subjects gave written informed consent for the MRI examination and the subsequent scientific evaluation of the data sets. The sample size was estimated according to Eng. Assuming an SD of 10 % and a minimum expected difference of 5 %, the sample size was calculated to be 7.85 [16].

MR imaging

A non-product single-shot spin-echo EPI sequence (multiband EPI: MB-EPI) capable of slice acceleration was modified to match a conventional WB-DWI protocol with a standard EPI sequence. This technology is also known as "multiband" or "simultaneous multi-slice." The slice-accelerated EPI sequence uses the blipped CAIPIRINHA technique to separate simultaneously excited slices and applies the GRAPPA (generalized autocalibrating partially parallel acquisition) reconstruction technique. The slice-acceleration factor, which is an integral factor and specifies the number of simultaneously excited slices, was set to 3.

All measurements were performed on a 3 T Siemens MRI scanner (MAGNETOM Skyra, Siemens Healthcare, Erlangen, Germany) using the complete whole-body matrix coil set (a 20-element head/neck matrix coil, a 32-element spine matrix coil, two 18-element body matrix coils, and a 36-element peripheral angio matrix coil). Subjects were placed in the supine position. The majority of imaging parameters were kept constant for both protocols: the whole-body examination contained seven blocks covering the body from head to toe. An overview of the imaging parameters is provided in **Table 1**. Differences between the two protocols were: (a) In the slice-accelerated EPI sequence, a slice-acceleration factor of 3 was applied; (b) this allowed for a notable reduction of the repetition time (TR) to 5000 ms, whereas the conventional EPI sequence had a minimum TR of 10 700 ms; (c) to keep the SNR stable, the high b-value of 800 s/mm^2 of the conventional WB-DWI protocol was reduced to 700 s/mm^2; (d) a slight increase of the echo time (TE) from 70 ms to 73 ms in the slice-accelerated EPI was noted; and (e) in the slice-accelerated EPI, the number of slices per acquisition block had to be increased from 50 to 51 (to reach a multiple of the applied slice-acceleration factor of 3). In both acquisition protocols and for all table positions, SPAIR fat saturation was applied with previous advanced automatic shimming. Parametric maps of the apparent diffusion coefficient (ADC)

This document was downloaded for personal use only. Unauthorized distribution is strictly prohibited.

scan parameter	slice-accelerated EPI	standard EPI
echo time (TE) [ms]	73	70
repetition time (TR) [ms]	5000	10 700
FOV [mm]	430x430	430x430
in-plane resolution [mm] (voxel size)	1.43x1.43	1.43x1.43
slice thickness [mm]	5	5
number of slices	51	50
bandwidth [Hz/px]	2085	2085
fat saturation	SPAIR	SPAIR
shim	advanced	advanced
in-plane parallel imaging	GRAPPA 2	GRAPPA 2
slice acceleration	factor 3	–
diffusion mode	trace, inverted	trace, inverted
b-values [s/mm^2]	0 (3 averages),	0 (3 averages),
	50 (2 averages),	50 (2 averages),
	700 (5 averages)	800 (5 averages)

Table 1 Scan parameters of slice-accelerated EPI and standard EPI.

Tab. 1 Messparameter der schichtbeschleunigten EPI und der Standard-EPI.

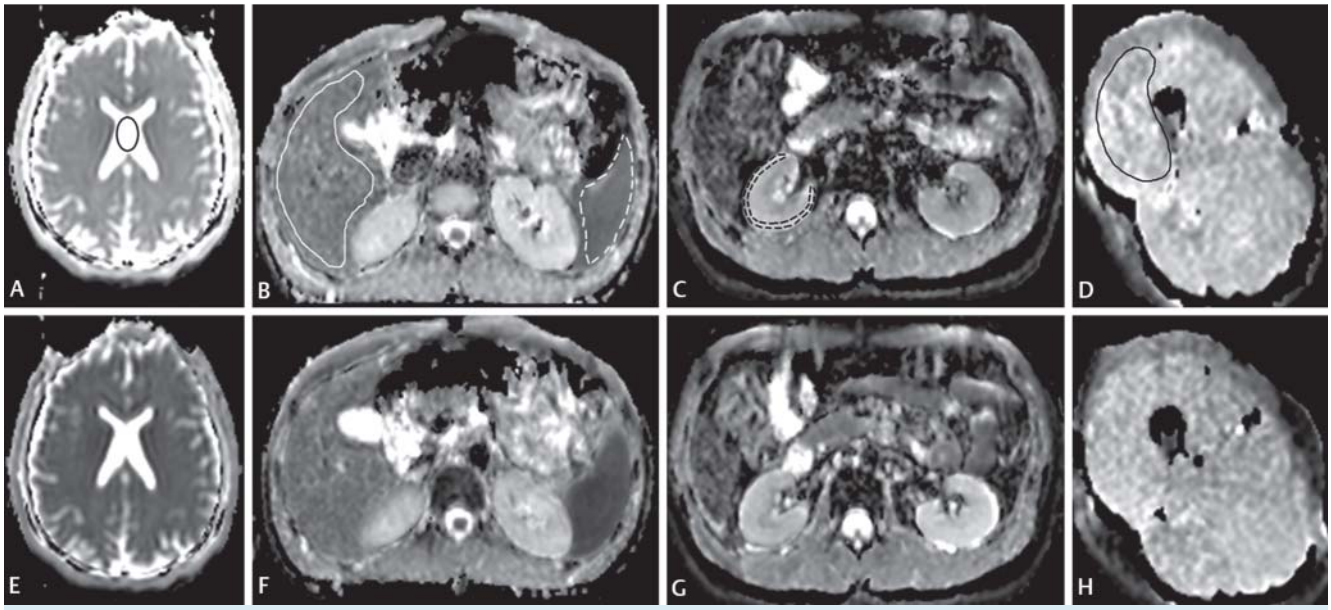

Fig. 1 This figure shows the ADC cross sections of MB-EPI **A–D** and standard EPI **E–H** at different levels: head **A, E**, abdomen **B, C, F, G** and upper leg **D, H**. The typical ROI placement for CSF (**A**: black line), liver (**B**: continuous white line), spleen (**B**: dashed white line), renal cortex (**C**: dashed black line) and muscle (**D**: continuous black line) is also shown.

Abb. 1 Die Abbildung zeigt die ADC-Schnittbilder der MB-EPI **A–D** und Standard-EPI **E–H** auf unterschiedlichen Höhen: Kopf **A, E**, Abdomen **B, C, F, G** und obere Extremität **D, H**. Die typische Platzierung der ROI für Liquor (**A**: Schwarze Linie), Leber (**B**: Kontinuierliche weisse Line), Milz (**B**: Gestrichelte weisse Linie), Nierenkortex (**C**: Gestrichelte schwarze Linie) Muskel (**D**: Kontinuierliche schwarze Linie) ist zu sehen.

were automatically calculated by the built-in post-processing routine. Furthermore, the head of one more volunteer was measured using the same b-value in both sequences (b = 800 s/mm^2).

Qualitative imaging evaluation

Image quality of the ADC maps and of the DWI trace images of the higher b-value (700 s/mm^2 for slice-accelerated EPI, 800 s/mm^2 for standard EPI sequence) and the lower b-value (50 s/mm^2 each) were assessed by two independent radiologists, one with 12 years and the other with 3 years of experience. We used the following 4-point Likert scale to rate the depiction of the white matter (WM), gray matter (GM), CSF, liver, spleen, renal cortex, renal medulla, and skeletal muscle on the ADC maps and trace maps: 1 (excellent), 2 (good), 3 (fair), 4 (poor). Furthermore, the overall level of image noise on ADC and trace maps was determined based on another 4-point scale for the head, abdomen, and upper leg: 1 (very little), 2 (little), 3 (moderate), 4 (severe).

Quantitative ROI analysis of ADC values

To assess the comparability and variability of the ADC values for both sequence types, we performed a region-of-interest (ROI) analysis of different parenchymal organs (CSF, WM, GM, liver, spleen, renal cortex, and muscle). The ROIs were placed as shown in **Fig. 1**.

Statistical analysis

For statistical analysis, the SPSS 22.0 software package (IBM SPSS Statistics, IBM Corp., Somers, NY) was used. The image quality scores of slice-accelerated DWI and conventional DWI were compared using multivariate ANOVA. A p-value of less than 0.05 was

This document was downloaded for personal use only. Unauthorized distribution is strictly prohibited.

considered significant. The mean and standard deviation of ADC values was calculated. ADC values for both imaging protocols were compared using the two-sided Student's *t*-test with Bonferroni correction after a Kolmogorov-Smirnov test was performed to test for normality. Furthermore, the coefficients of variation (CVs) of the ADC values for both sequences were calculated by dividing the standard deviations by the mean values for the above-mentioned tissues. The inter-rater reliability was analyzed by calculating the intra-class correlation coefficient (ICC). The ICC values have been interpreted according to Kundel et al. [17]: Values of 0.81 – 1.00 indicate almost perfect agreement; 0.61 – 0.80 substantial agreement; 0.41 – 0.60 moderate agreement; 0.21 – 0.40 fair agreement; and less than 0.21 poor agreement.

Results

Acquisition time

A substantial reduction in scan acquisition time could be achieved using the slice-accelerated EPI sequence (**Fig. 2**). For four table positions (from head to upper thigh), a time reduction of 24.2 % (26:08 instead of 34:29) could be achieved, and for a whole-body protocol with 7 table positions, a time reduction of 25.9 % (41:13 instead of 55:37) could be achieved. **Table 2, 3** give a comprehensive overview of the acquisition times for each block and the influence of the shimming, diffusion sequence, and prescans on the acquisition times. The estimated acquisition times include more than the real diffusion sequence, e. g., single-band dummy scans, in-plane reference scans, simultaneous multi-slice (SMS) reference

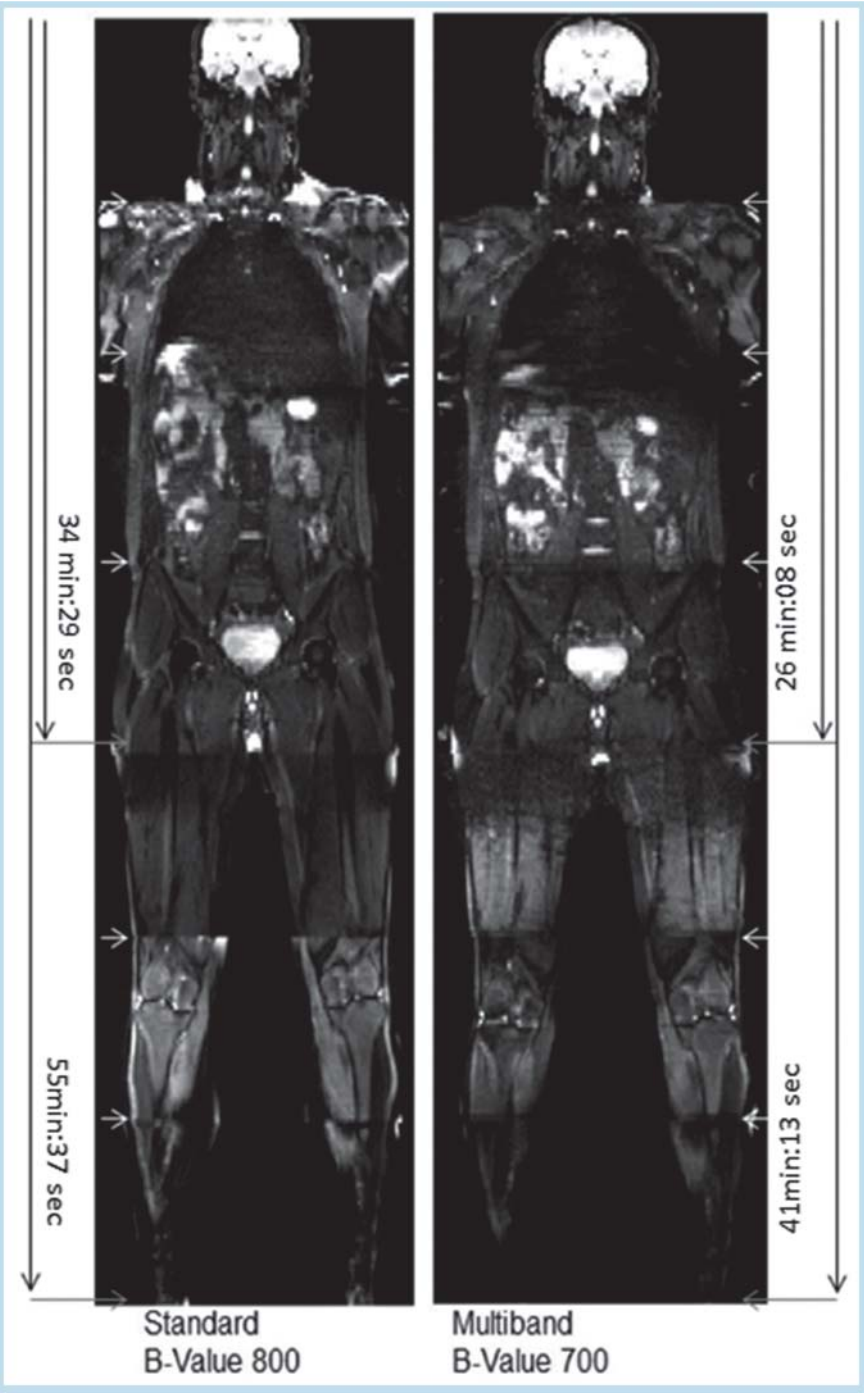

Fig. 2 This figure shows the trace-weighted whole-body images from the slice-accelerated EPI sequence and the standard EPI and compares the measurement times of slice-accelerated EPI (right) and standard EPI (left): The shorter time indicates the acquisition time of 4 blocks (body without extremities) and the longer time indicates the time of acquisition of 7 blocks (whole body). The grey and white arrows show each block.

Abb. 2 Diese Abbildung zeigt die Trace-weighted Ganzkörper-Aufnahmen der schichtbeschleunigten EPI-Sequenz und die Standard-EPI und vergleicht die Messzeit von der schichtbeschleunigten EPI-Sequenz (rechts) und der Standard-EPI (links): Die kürzere Zeit zeigt die Akquisition von 4 Blöcken (Körper ohne Extremitäten) und die längere Zeit zeigt die Messzeit von 7 Blöcken (Ganzkörper). Die grauen und weissen Pfeile zeigen jeden Block.

This document was downloaded for personal use only. Unauthorized distribution is strictly prohibited.

Table 2 Influence of the shimming, diffusion sequence, and prescans on the acquisition time for each block for the slice-accelerated sequence.

Tab. 2 Einfluss des Shimming, der Diffusionssequenz und der Prescans auf die Messzeit für jeden gemessenen Block für die schichtbeschleunigte EPI-Sequenz.

accelerated slice	measured time (min:sec)	estimated time (Siemens) (min:sec)	diffusion duration (min:sec)	prescans duration (reference scans and dummy scans) (min:sec)	difference caused by shimming (min:sec)
block 1	4:55	2:21	2:00	0:21	2:34
block 2	5:12	2:21	2:00	0:21	2:51
block 3	5:11	2:21	2:00	0:21	2:50
block 4	4:55	2:21	2:00	0:21	2:34
block 5	5:05	2:21	2:00	0:21	2:44
block 6	5:00	2:21	2:00	0:21	2:39
block 7	5:00	2:21	2:00	0:21	2:39

Table 3 Influence of the shimming, diffusion sequence, and prescans on the acquisition time for each block for the standard sequence.

Tab. 3 Einfluss des Shimming, der Diffusionssequenz und der Prescans auf die Messzeit für jeden gemessenen Block für die Standard-EPI-Sequenz.

standard sequence	measured time (min:sec)	estimated time (Siemens) (min:sec)	diffusion duration (min:sec)	prescans duration (min:sec)	difference caused by shimming (min:sec)
block 1	7:02	4:17	4:17	0	2:45
block 2	7:07	4:17	4:17	0	2:50
block 3	7:22	4:17	4:17	0	3:05
block 4	7:03	4:17	4:17	0	2:46
block 5	7:03	4:17	4:17	0	2:46
block 6	7:03	4:17	4:17	0	2:46
block 7	7:03	4:17	4:17	0	2:46

scans, SMS dummy scans, and eddy current reference scans. The function of the dummy scans is to reach the steady state, i. e., to achieve the intended flip angle by repeated excitation with magnetization remaining from the previous excitation. The reference scans are needed to split the measured slice-accelerated data, the in-plane reference scan is needed for the calculation of the kernel of unmeasured k-space values, and the SMS reference scan is needed for the separation of simultaneously excited slices. The reference scans are applied in the following order: 1. Dummy scan (a single-band scan with the total amount of slices); 2. SMS reference scan; 3. In-plane reference scan; 4. SMS dummy scan. The duration of reference scans 2, 3, and 4 is shorter than that of reference scan 1 because of the acceleration factor used. In this study, an acceleration factor of 3 was used. Therefore, the estimated duration of the image acquisition for each block is greater than that which is calculated using the following equation: Time of acquisition = (Time for reference and dummy scans) + TR × gradient directions × (sum of averages for different b-values > 0) + TR × (averages for b-value = 0).

When applying this equation to our study, the time for the slice-accelerated sequence is: Time of acquisition = (10.7 sec + (10.7 sec/slice-acceleration factor of 3) × 3 prescans) + 5 sec (TR) × 3 (gradient directions) × 7 (sum of averages for different b-values > 0) + 5 sec (TR) × 3 (averages for b-value = 0) = 141.4 sec.

When applying this equation to our study, the time for the standard sequence is: Time of acquisition = 10.7 sec (TR) × 3 (gradient directions) × 7 (sum of averages for different b-values > 0) + 10.7 sec (TR) × 3 (averages for b-value = 0) = 256.8 sec.

Table 4 Results of the readout of the trace-weighted images (b = 50 s/mm²) showing the mean values for image quality and the noise of different body regions.

Tab. 4 Ergebnisse des Readout der TRACE-gewichteten Bilder (b = 50 s/mm²). Dargestellt sind der Mittelwert der Bilddarstellung und des Rauschens für unterschiedliche Körperregionen.

organ	slice-accelerated EPI		standard EPI	
	reader 1	reader 2	reader 1	reader 2
	mean ± SD	mean ± SD	mean ± SD	mean ± SD
CSF	2.3 ± 0.5	2.3 ± 0.5	2.1 ± 0.4	2.1 ± 0.4
GM	2.0 ± 0.0	2.1 ± 0.4	2.1 ± 0.4	2.0 ± 0.0
WM	2.3 ± 0.5	2.3 ± 0.5	2.1 ± 0.4	2.3 ± 0.5
head noise	1.1 ± 0.4	1.0 ± 0.0	1.0 ± 0.0	1.0 ± 0.0
liver	2.5 ± 0.5	2.6 ± 0.5	2.3 ± 0.5	2.3 ± 0.5
kidney	2.1 ± 0.4	2.0 ± 0.0	2.0 ± 0.0	2.0 ± 0.0
RC	2.3 ± 0.5	2.0 ± 0.0	2.0 ± 0.0	2.0 ± 0.0
RM	2.0 ± 0.0	2.0 ± 0.0	2.0 ± 0.0	2.0 ± 0.0
spleen	2.1 ± 0.4	2.0 ± 0.0	2.3 ± 0.5	2.1 ± 0.4
abdomen noise	1.3 ± 0.5	1.3 ± 0.5	1.4 ± 0.5	1.4 ± 0.5
muscle	2.1 ± 0.4	2.0 ± 0.0	2.3 ± 0.5	2.3 ± 0.5
muscle noise	2.1 ± 0.4	2.1 ± 0.4	2.1 ± 0.4	2.0 ± 0.0

Scale used for rating image quality: 1 (excellent), 2 (good), 3 (fair), 4 (poor). Scale used for rating noise level: 1 (very little), 2 (little), 3 (moderate), 4 (severe).
Die Skala für die Bildqualität war: 1 (Exzellente Darstellung), 2 (Gute Darstellung), 3 (Ausreichende Darstellung), 4 (Schwache Darstellung). Die Skala für das Rauschen war: 1 (Sehr wenig Rauschen), 2 (Wenig Rauschen), 3 (Mässiges Rauschen), 4 (Starkes Rauschen).

Qualitative image evaluation

Both methods showed subjectively comparable image quality with good to fair depiction of anatomical structures and little to moderate noise, depending on the imaging region. **Table 4 – 6** summarize the results of the readout showing the mean values for organ image quality and the noise level of different regions. The intra-class correlation coefficient (ICC) indicated almost perfect agreement on the b = 50 s/mm² images, with an ICC of 0.87 on the slice-accelerated images and 0.95 on the standard EPI se-

This document was downloaded for personal use only. Unauthorized distribution is strictly prohibited.

Table 5 Results of the readout of the trace-weighted images (b = 700 s/mm² and b = 800 s/mm²) showing the mean values for image quality and the noise of different body regions.

Tab. 5 Ergebnisse des Readout der TRACE-gewichteten Bilder (b = 700 s/mm² und b = 800 s/mm²). Dargestellt sind der Mittelwert der Bilddarstellung und des Rauschens für unterschiedliche Körperregionen.

organ	slice accelerated-EPI		standard EPI	
	reader 1	reader 2	reader 1	reader 2
	mean ± SD	mean ± SD	mean ± SD	mean ± SD
CSF	2.4 ± 0.5	2.3 ± 0.5	2.3 ± 0.5	2.3 ± 0.5
GM	2.0 ± 0.0	2.4 ± 0.5	2.1 ± 0.4	2.3 ± 0.5
WM	2.1 ± 0.4	2.4 ± 0.5	2.1 ± 0.4	2.3 ± 0.5
head noise	1.1 ± 0.4	1.0 ± 0.0	1.0 ± 0.0	1.0 ± 0.0
liver	2.5 ± 0.5	2.5 ± 0.5	2.3 ± 0.5	2.3 ± 0.5
kidney	2.0 ± 0.0	2.0 ± 0.0	2.0 ± 0.0	2.0 ± 0.0
RC	2.0 ± 0.0	2.0 ± 0.0	2.0 ± 0.0	2.0 ± 0.0
RM	2.0 ± 0.0	2.0 ± 0.0	2.0 ± 0.0	2.0 ± 0.0
spleen	2.1 ± 0.4	2.1 ± 0.4	2.1 ± 0.4	2.1 ± 0.4
abdomen noise	1.4 ± 0.7	1.3 ± 0.5	1.4 ± 0.5	1.4 ± 0.5
muscle	2.4 ± 0.7	2.3 ± 0.7	2.3 ± 0.5	2.3 ± 0.5
muscle noise	2.3 ± 0.7	2.3 ± 0.7	2.1 ± 0.4	2.1 ± 0.4

Scale used for rating image quality: 1 (excellent), 2 (good), 3 (fair), 4 (poor). Scale used for rating noise level: 1 (very little), 2 (little), 3 (moderate), 4 (severe).
Die Skala für die Bildqualität war: 1 (Exzellente Darstellung), 2 (Gute Darstellung), 3 (Ausreichende Darstellung), 4 (Schwache Darstellung). Die Skala für das Rauschen war: 1 (Sehr wenig Rauschen), 2 (Wenig Rauschen), 3 (Mässiges Rauschen), 4 (Starkes Rauschen).

Table 6 Results of the readout of the ADC maps showing the mean values for image quality and the noise of different body regions.

Tab. 6 Ergebnisse des Readout der ADC-Maps. Dargestellt sind der Mittelwert der Bilddarstellung und des Rauschens für unterschiedliche Körperregionen.

organ	slice accelerated-EPI		standard EPI	
	reader 1	reader 2	reader 1	reader 2
	mean ± SD	mean ± SD	mean ± SD	mean ± SD
CSF	2.0 ± 0.0	2.0 ± 0.0	2.0 ± 0.0	2.0 ± 0.0
GM	2.8 ± 0.5	2.9 ± 0.4	2.5 ± 0.5	2.5 ± 0.5
WM	2.8 ± 0.5	3.0 ± 0.0	2.5 ± 0.5	2.3 ± 0.5
head noise	2.3 ± 0.5	2.3 ± 0.5	2.6 ± 0.5	3.0 ± 0.0
liver	3.3 ± 0.5	3.4 ± 0.5	2.8 ± 0.5	3.0 ± 0.5
kidney	2.2 ± 0.4	2.2 ± 0.4	2.1 ± 0.4	2.3 ± 0.5
RC	2.6 ± 0.7	2.9 ± 0.6	2.6 ± 0.5	2.8 ± 0.5
RM	2.6 ± 0.7	2.9 ± 0.6	2.6 ± 0.5	2.8 ± 0.5
spleen	2.5 ± 0.8	2.3 ± 0.5	2.3 ± 0.5	2.3 ± 0.5
abdomen noise	2.4 ± 0.7	2.3 ± 0.5	3.0 ± 0.8	2.9 ± 0.4
muscle	3.9 ± 0.4	4.0 ± 0.0	3.9 ± 0.4	3.8 ± 0.5
muscle noise	2.8 ± 0.7	3.1 ± 0.4	2.3 ± 0.7	2.5 ± 0.8

Scale used for rating image quality: 1 (excellent), 2 (good), 3 (fair), 4 (poor). Scale used for rating noise level: 1 (very little), 2 (little), 3 (moderate), 4 (severe).
Die Skala für die Bildqualität war: 1 (Exzellente Darstellung), 2 (Gute Darstellung), 3 (Ausreichende Darstellung), 4 (Schwache Darstellung). Die Skala für das Rauschen war: 1 (Sehr wenig Rauschen), 2 (Wenig Rauschen), 3 (Mässiges Rauschen), 4 (Starkes Rauschen).

quence. Furthermore, the ANOVA showed no significant differences between the sequence (p = 0.54) and the reader (p = 0.38) on these images. On the images with high b-values, the ICC also indicated almost perfect agreement, with 0.84 on the slice-accelerated images and 0.96 on the standard EPI sequence. The ANOVA revealed no significant differences between reader (p = 0.62) and sequence (p = 0.55). On the ADC maps there were also no differences between reader (p = 0.054) and sequence (p = 0.33), and the ICC further indicated almost perfect agreement on the slice-accelerated (0.83) and the standard EPI images (0.81).

The liver and muscle showed a significantly poorer depiction compared to the kidney, and upper leg noise was significantly higher compared to head noise. The liver and muscle are located close to air, leading to susceptibility differences at air-tissue interfaces, which might explain the above-mentioned differences. Additionally, artifacts due to severe tissue motion could explain the poorer depiction of the liver.

Quantitative assessment of ADC values

The measured ADC values and the coefficients of variation (CVs) are summarized in **Table 7**. No significant differences in the ADC values for the two sequences were found for the parenchymal abdominal organs, CSF, and skeletal muscle: liver p = 0.3; renal cortex p = 0.4; spleen p = 0.5; CSF p = 0.7; and skeletal muscle p = 0.2. However, GM and WM showed higher ADC values for the slice-accelerated protocol (p < 0.01 for both GM and WM).

This finding was confirmed in the measurements in one volunteer using identical b-values.

The CVs of the ADC values of CSF, GM and WM were lower in the protocol using the slice-accelerated EPI sequence than in the standard protocol, whereas the CVs of parenchymal abdominal organs and skeletal muscle were higher in the slice-acceleration approach when compared to the standard protocol.

Preliminary assessment of clinical applicability in one patient

Slice-accelerated WB-DWI measurement in one patient with metastatic renal cell carcinoma was successfully performed (**Fig. 3**). The known metastatic lesions (pulmonary metastases, metastasis in the right flank) could easily be identified. The detected lesions exhibited ADC values ranging from 1.32 (±0.23) × 10^{-3} mm²/s for the pulmonary metastasis to 1.27 (±0.01) × 10^{-3} mm²/s for the flank metastasis.

Discussion

The application of whole-body diffusion-weighted imaging (WB-DWI) in the clinical workup of oncological patients is severely hampered by the long acquisition time of conventional protocols. In the present study, we demonstrated that the new technique of simultaneous multi-slice excitation and data readout in diffusion-weighted EPI sequences can be applied to significantly reduce measurement time. Furthermore, we did not detect significant differences in image quality, and, for the most part, the ADC values were not significantly different from those for conventional EPI sequences.

In our protocol, we were able to reduce overall measurement time for whole-body acquisition by 24.2 – 25.9 % using a slice-acceleration factor of 3. In principle, the acceleration factor correlates to a directly proportional reduction in measurement time; therefore, with an acceleration factor of 2 the acquisition time can be reduced by 50 %. The reason for the smaller reduction in measurement time in our protocol is the time needed for advanced shimming at each table position. We were not able to obtain sufficient image quality using an inversion prepulse for fat saturation in our sequence in development. To obtain satisfactory fat suppression in areas of strong magnetic field inhomogeneities

This document was downloaded for personal use only. Unauthorized distribution is strictly prohibited.

mean and standard deviation of ADC values, coefficients of variation			
organ	**slice-accelerated EPI ADC [x10^{-3} mm^2/s], CV**	**standard EPI ADC [x10^{-3} mm^2/s], CV**	**literature reference ADC [x10^{-3} mm^2/s]**
GM	0.92 ± 0.03, 3.1 %	0.67 ± 0.02, 3.5 %	0.93 ± 0.15 [21]
WM	1.04 ± 0.02, 1.9 %	0.79 ± 0.03, 3.8 %	0.76 ± 0.05 to 0.9 ± 0.11 [18]
CSF	2.91 ± 0.30, 10.3 %	2.87 ± 0.31, 10.7 %	3.06 ± 0.19 [21]
liver	1.20 ± 0.17, 14.5 %	1.13 ± 0.08, 6.7 %	1.28 ± 0.12 [20]
renal cortex	2.07 ± 0.22, 10.5 %	2.12 ± 0.10, 4.7 %	2.26 ± 0.37 [19]
spleen	1.10 ± 0.18, 17.9 %	0.96 ± 0.07, 7.2 %	0.81 ± 0.13 [20]
skeletal muscle	1.59 ± 0.10, 6.2 %	1.54 ± 0.06, 3.8 %	1.77 ± 0.36 [21]

Table 7 Mean and standard deviation of ADC values, coefficients of variation of slice-accelerated EPI and standard EPI of different organs.

Tab. 7 Mittelwert und Standardabweichung der ADC-Werte, Variationskoeffizient der schichtbeschleunigten EPI und der Standard-EPI von unterschiedlichen Organen.

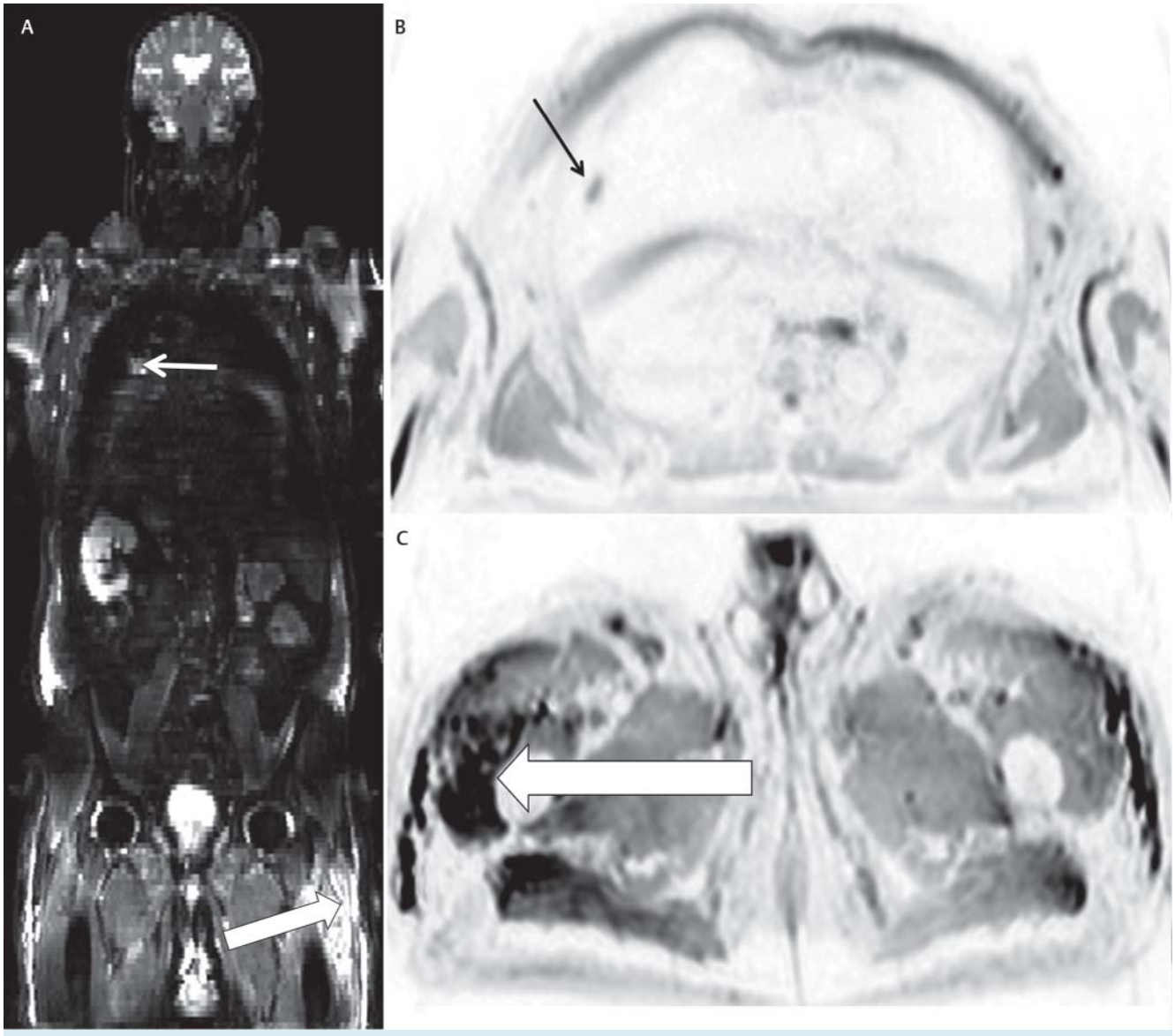

Fig. 3 This figure shows the MB-EPI trace-weighted inverted images of a 74-year-old patient with metastatic renal cell carcinoma, specifically with pulmonary metastases (**A**: thin white arrow; **B**: black arrow) and a metastasis in the vastus lateralis (**A**: thick white arrow; **C**: white arrow). The coronal images are not inverted but the axial images are. The patient had undergone left-sided nephrectomy and resection of the pancreas.

Abb. 3 Diese Abbildung zeigt die MB-EPI Trace-weighted invertierten Bilder eines 74-jährigen Patienten mit einem metastasierten Nierenzellkarzinom mit pulmonalen Metastasen (**A** dünner weisser Pfeil und **B** schwarzer Pfeil) und einer Metastase im vastus lateralis (**A** dicker weisser Pfeil und **C** weisser Pfeil). Die koronaren Bilder sind nicht invertiert und die axialen sind invertiert. Der Patient hatte eine Nephrektomie links und eine Resektion vom Pankreas.

This document was downloaded for personal use only. Unauthorized distribution is strictly prohibited.

such as the neck area, we had to apply a time-consuming advanced automatic shim routine combined with SPAIR fat suppression. Switching the shim from the advanced routine to a standard technique would lead to a reduction in scanning time of 35 – 54 %. There is no technical reason precluding the application of an inversion pulse to the simultaneous multi-slice acquisitions, which should be possible with further development of the slice-accelerated EPI sequence.

Although we were able to achieve comparable image quality and similar quantitative ADC values for both protocols, statistically significant differences remained. The most prominent difference is the higher ADC values for the slice-accelerated acquisition measured in brain tissue. We initially thought that this finding may be attributed to the slightly different high b-value that was applied in the multiband slice-accelerated acquisition. Therefore, the head of another volunteer was scanned using the slice-accelerated sequence with a b-value of 800 s/mm^2 and using the standard sequence. However, using the same b-value does not cause a change that explains the statistically significant difference we observed in the brain tissue. The slice-accelerated acquisition leads to a slight reduction in signal-to-noise ratio (the exact SNR quantification was out of the scope of our study) compared to the standard EPI sequence, e. g., due to a reduction in repetition time. We tried to compensate for this loss in SNR by adjusting the b-value from 800 s/mm^2 to 700 s/mm^2. A stronger b-value results in decreased SNR due to stronger signal dephasing caused by the diffusion gradients. We observed a decrease of the SNR of the multiband sequence compared to that of the standard EPI sequence when using the same b-value. However, since our goal was to keep the SNR stable, we changed the b-value in the multiband sequence, which might have slightly affected the DWI contrast. The remaining ADC values and CVs were in the range of previously reported literature values [18 – 21].

The faster acquisition potentially allows the use of diffusion imaging methods with longer acquisition times in whole-body imaging, e. g., intravoxel incoherent motion and diffusion kurtosis imaging in a clinically applicable measurement time.

We were only able to provide preliminary data on the clinical applicability with the evaluation of one patient with metastatic disease. In this single examination, the detectability of the metastatic lesions was in the expected range. However, the applicability of the slice-accelerated EPI sequence for different oncological diseases has to be further evaluated.

In conclusion, slice-accelerated EPI greatly reduces measurement time without having a significant impact on image quality. The reduction in measurement time might strongly contribute to the clinical applicability of WB-DWI. However, further refinement of the slice-accelerated EPI sequence and the WB-DWI protocol applying this sequence type seems necessary, and the value of such WB-DWI protocols for assessment of systemic oncological diseases needs to be investigated in further clinical studies.

Erratum (2.2.2016): Kenkel D, Wurnig MC, Filli L. Whole-Body Diffusion Imaging Applying Simultaneous Multi-Slice Excitation. Fortschr Röntgenstr 2016; DOI: 10.1055/s-0035-1567032

The authors name Wurmig MC and Ulbrich EJ was changed. On the 1st and the 2nd page, the correct abbreviation of the "controlled aliasing in parallel imaging results in higher acceleration" technique is CAIPIRINHA.

References

1 *Gu J, Chan T, Zhang J et al.* Whole-Body Diffusion-Weighted Imaging: The Added Value to Whole-Body MRI at Initial Diagnosis of Lymphoma. American Journal of Roentgenology 2011; 197: W384 – W391
2 *Giles SL, Messiou C, Collins DJ et al.* Whole-Body Diffusion-weighted MR Imaging for Assessment of Treatment Response in Myeloma. Radiology 2014; 271: 785 – 794
3 *Petralia G, Padhani A, Summers P et al.* Whole-body diffusion-weighted imaging: is it all we need for detecting metastases in melanoma patients? Eur Radiol 2013; 23: 3466 – 3476
4 *Nagamachi S, Wakamatsu H, Kiyohara S et al.* Comparison of diagnostic and prognostic capabilities of 18F-FDG-PET/CT, 131I-scintigraphy, and diffusion-weighted magnetic resonance imaging for postoperative thyroid cancer. Jpn J Radiol 2011; 29: 413 – 422
5 *Lambregts DMJ, Maas M, Cappendijk VC et al.* Whole-body diffusion-weighted magnetic resonance imaging: Current evidence in oncology and potential role in colorectal cancer staging. European Journal of Cancer 2011; 47: 2107 – 2116
6 *Chen Y, Hu C, Chen G et al.* Staging of uterine cervical carcinoma: whole-body diffusion-weighted magnetic resonance imaging. Abdom Imaging 2011; 36: 619 – 626
7 *Akay S, Kocaoglu M, Emer O et al.* Diagnostic accuracy of whole-body diffusion-weighted magnetic resonance imaging with 3.0 T in detection of primary and metastatic neoplasms. Journal of Medical Imaging and Radiation Oncology 2013; 57: 274 – 282
8 *Del Vescovo R, Frauenfelder G, Giurazza F et al.* Role of whole-body diffusion-weighted MRI in detecting bone metastasis. Radiol med 2014: 1 – 9
9 *Li B, Li Q, Nie W et al.* Diagnostic value of whole-body diffusion-weighted magnetic resonance imaging for detection of primary and metastatic malignancies: A meta-analysis. European Journal of Radiology 2014; 83: 338 – 344
10 *Mayerhoefer ME, Karanikas G, Kletter K et al.* Evaluation of Diffusion-Weighted MRI for Pretherapeutic Assessment and Staging of Lymphoma: Results of a Prospective Study in 140 Patients. Clinical Cancer Research 2014; 20: 2984 – 2993
11 *Mosavi F, Johansson S, Sandberg DT et al.* Whole-Body Diffusion-Weighted MRI Compared With 18F-NaF PET/CT for Detection of Bone Metastases in Patients With High-Risk Prostate Carcinoma. American Journal of Roentgenology 2012; 199: 1114 – 1120
12 *Glover GH.* Phase-offset multiplanar (POMP) volume imaging: a new technique. J Magn Reson Imaging 1991
13 *Breuer FA, Blaimer M, Heidemann RM et al.* Controlled aliasing in parallel imaging results in higher acceleration (CAIPIRINHA) for multi-slice imaging. Magnetic Resonance in Medicine 2005; 53: 684 – 691
14 *Setsompop K, Gagoski BA, Polimeni JR et al.* Blipped-controlled aliasing in parallel imaging for simultaneous multislice echo planar imaging with reduced g-factor penalty. Magnetic Resonance in Medicine 2012; 67: 1210 – 1224
15 *Himanshu JC, Cornfeld D, Strecker R et al.* Accelerated diffusion weighted imaging in the liver with blipped CAIPIRINHA based simultaneous multi slice acquisition. Proc Intl Soc Mag Reson Med 2013; 21
16 *Eng J.* Sample Size Estimation: How Many Individuals Should Be Studied? Radiology 2003: 309 – 312
17 *Kundel HL, Polansky M.* Measurement of Observer Agreement. Radiology 2003; 228: 303 – 308
18 *García Santos JM, Ordóñez C, Torres del Río S.* ADC measurements at low and high b values: insight into normal brain structure with clinical DWI. Magnetic Resonance Imaging 2008; 26: 35 – 44
19 *Gürses B, Kiliçkesmez O, Taşdelen N et al.* Diffusion tensor imaging of the kidney at 3 Tesla MRI: normative values and repeatability of measurements in healthy volunteers. Diagnostic and Interventional Radiology 2011; 17: 317 – 322
20 *Rosenkrantz AB, Geppert C, Kiritsy M et al.* Diffusion-weighted imaging of the liver: comparison of image quality between monopolar and bipolar acquisition schemes at 3T. Abdom Imaging 2014
21 *Filli L, Wurnig M, Nanz D et al.* Whole-Body Diffusion Kurtosis Imaging: Initial Experience on Non-Gaussian Diffusion in Various Organs. Investigative Radiology 9000; Publish Ahead of Print:10.1097/RLI.0000000000000082

This document was downloaded for personal use only. Unauthorized distribution is strictly prohibited.